Available online at www.sciencedirect.com
ScienceDirect
Science and Technology of Advanced Materials 8 (2007) 237–248
SCIENCE AND TECHNOLOGY OF ADVANCED MATERIALS
www.elsevier.com/locate/stam

Microstructural characterization of Mg–Al–Sr alloys

M. Aljarrah[a], M.A. Parvez[a], Jian Li[b], E. Essadiqi[b], M. Medraj[a,*]

[a]*Department of Mechanical Engineering, Concordia University, 1455 de Maisonneuve Blvd. West, Montreal, Que., Canada H3G 1M8*
[b]*CANMET-MTL, 580 Booth Street, Ottawa, Ont., Canada K1A 0E4*

Received 13 October 2006; received in revised form 19 January 2007; accepted 29 January 2007
Available online 6 March 2007

Abstract

The microstructural details of fourteen Mg–Al–Sr alloys were investigated in the as-cast form by a combination of scanning electron microscopy/energy dispersive spectrometer (SEM/EDS) analysis and quantitative electron probe microanalysis (EPMA). The heat transfer method coupled with the DSC measurement has been utilized to determine the solidification curves of the alloys. The morphology and the chemical composition of the phases were characterized. The microstructure of the alloys is primarily dominated by (Mg) and (Al_4Sr). In the present investigation, ternary solid solubility of three binary compounds extended into the ternary system has been reported and denoted as: (Al_4Sr), ($Mg_{17}Sr_2$) and ($Mg_{38}Sr_9$). The (Al_4Sr) phase is a substitutional solid solution represented by $Mg_xAl_{4-x}Sr$ and has a plate-like structure. The maximum solubility of Al in $Mg_{17}Sr_2$ was found to be 21.3 at%. It was also observed that $Mg_{38}Sr_9$ dissolved 12.5 at% Al.

Keywords: Mg–Al–Sr; Microstructure; Solidification curves; Ternary solubility

1. Introduction

The interest in Magnesium-based alloys is continuously increasing, especially because of their applications in the transportation industry for weight reduction and the consequent increased fuel efficiency [1,2]. However, magnesium alloys face a challenge at higher temperature application because of their limited creep properties. In recent years, Mg–Al–Sr alloy system has emerged as a potential system for heat-resistant Mg-alloys [3]. Noranda developed alloys based on the Mg–Al–Sr system, which are being used by BMW for the manufacturing of die-cast engine blocks [4].

Within the ternary Mg–Al–Sr system, there is a huge amount of possibilities to select alloy compositions. Wrought magnesium, particularly in the form of sheet, represents a tremendous growth opportunity in magnesium alloys applications. Significant improvement in creep resistance has been achieved. But the phase relations and phase stability under given conditions can be better understood through microstructural characterization. To date, little effort has been made to construct the phase relationships of the Mg–Al–Sr system. The published experimental works on the phase equilibria of the Mg–Al–Sr system are self-contradictory. Prince et al. [5] summarized the work done on the Mg–Al–Sr system. The experimental work on the phase equilibria of the Mg–Al–Sr system was primarily originated by Makhmudov and coworkers in early 1980s [6–10]. However, inconsistency was noticed between their works. Makhmudov et al. [8], also, reported a ternary compound with stoichiometry of $Al_{34}Mg_6Sr_{60}$ (Al_6MgSr_{10}), which is different from the earlier reported X compound. The solubility limits for the binary compounds determined by Makhmudov et al. [9] do not agree with the 400 °C isothermal section given by Makhmudov et al. [8] in 1981. Prince et al. [5] developed a tentative liquidus surface using the experimental results from Refs. [7–10] with some disagreements in identifying the invariant points. Baril et al. [11] investigated four samples in the Mg-rich region of the Mg–Al–Sr system and tentatively designated a ternary phase as $Al_3Mg_{13}Sr$. In their work, the stoichiometry is not

*Corresponding author. Tel.: +1 514 848 2424x3146; fax: +1 514 848 3175.
E-mail address: mmedraj@encs.concordia.ca (M. Medraj).
URL: http://www.me.concordia.ca/~mmedraj.

1468-6996/$ - see front matter © 2007 NIMS and Elsevier Ltd. All rights reserved.
doi:10.1016/j.stam.2007.01.003

clearly identified and the chemical composition is not compatible with the ternary compound $Al_{34}Mg_6Sr_{60}$ reported by Makhmudov et al. [8]. Jing et al. [12] recently investigated the microstructure and tensile creep behavior of Mg–Al–Sr (AJ) based alloys and reported that a ternary interphase exists in the alloys containing 2–3 wt% Sr at the grain boundaries. Czerwinski and Zielinska-Lipiec [13] investigated the microstructural evolution of a Mg_5Al_2Sr (wt%) alloy and reported that the common feature of Sr-containing phases in the as-cast ingots is their location at grain or sub-grain boundaries. The presence of $Mg_{17}Al_{12}$ suggests an insufficient amount of Sr to bind all Al. At the same time, however, Sr reacted exclusively with Mg forming $Mg_{17}Sr_2$. Hence, it is very likely that the local segregation of Al and Sr led to a variety of phases. Chartrand and Pelton [14] reviewed and calculated the thermodynamic properties of the Mg–Al–Sr ternary and related binary sub-systems. No ternary terms were added to the thermodynamic model due to the uncertainties related to the existence, stability, homogeneity range and the melting and decomposition temperatures of the ternary compounds. In 2003, Koray et al. [15] calculated the liquidus projection of the ternary Mg–Al–Sr system that is very similar to Chartrand and Pelton's [14] calculation except for the narrower phase field of Mg_2Sr. The calculated phase diagram of [14,15] exhibited substantial disagreement with the experimental data. The extended solubilities between the solid phases were not considered in the thermodynamic assessment. Makhmudov et al. [6–10] reported an isothermal section at 400 °C [9] that shows a triangulation involving (Mg), $Mg_{17}Sr_2$ and γ phase. This seems unlikely, as the thermodynamic stabilities of these compounds are lower than Al_4Sr and Al_2Sr at this temperature. Further, the thermodynamic optimization of Chartrand and Pelton [14] shows that these compounds are in triangulation with Al_2Sr. From these discrepancies, it is believed that these thermodynamic evaluations of the ternary system should be revised. Besides, in the experimental work of Makhmudov et al. [9], the binary compound $Mg_{38}Sr_9$ was not included in the Mg–Al–Sr phase diagram. In 2004, Liu et al. [16] reported the potential existence of Al_3Sr_8 and Al_5Sr_4 compounds. Considering these compounds in the thermodynamic model will definitely alter the phase equilibria of the Mg–Al–Sr ternary diagram. A considerable discrepancy among the published results and very few experimental data demands new investigation for this system. This article presents solidification curves deduced from the DSC measurement, SEM/EDS and EPMA analyses to identify the phases in the Mg–Al–Sr system and to determine their compositions and answers many questions that were raised in previous articles [17–19].

2. Experimental

Fourteen alloys were chosen by critical assessment of the experimental and thermodynamic datasets that are available in the literature. Table 1 lists the different groups with the number of compositions and their phase fields that were predicted by thermodynamic calculations based on the model of Chartrand and Pelton [14]. Special attention was directed to the Mg-rich corner because of the interest in the Mg alloys. In order to study the phase triangulations of Al_4Sr and $Mg_{17}Sr_2$ with Mg and Al_4Sr with Mg and γ, samples containing this phase were also chosen. This will help in determining the extent of the $Mg_{17}Sr_2$ and Al_4Sr phase fields.

Mg–Al–Sr alloys were prepared by melting stoichiometric amounts of the constituent elements in an induction-melting furnace under argon with 1%SF_6 (sulfur hexafluoride) to protect the melt from oxidation. In preparing the alloys, magnesium of 99.8 wt%, aluminum of 99.9 wt% and strontium of 99 wt% were used. The isothermal section of the Mg–Al–Sr system, based on the work of [14], at room temperature with the investigated compositions in weight percentage is given in Fig. 1. The actual chemical composition was measured quantitatively by ICP atomic emission spectrometry. The loss in total mass was below 2% for most of the samples.

Table 1
The studied samples with the corresponding phase field

Group	Sample nos.	Predicted phases [14]
#1	1, 2,3,4,5,6,7	$Mg + Al_4Sr + \gamma$
#2	8,9	$Mg + Al_2Sr + Al_4Sr$
#3	10,11	$Al_4Sr + \gamma + \beta$
#4	12	$Al + Al_4Sr + \beta$
#5	13,14	$Mg + Al_2Sr + Mg_{17}Sr_2$

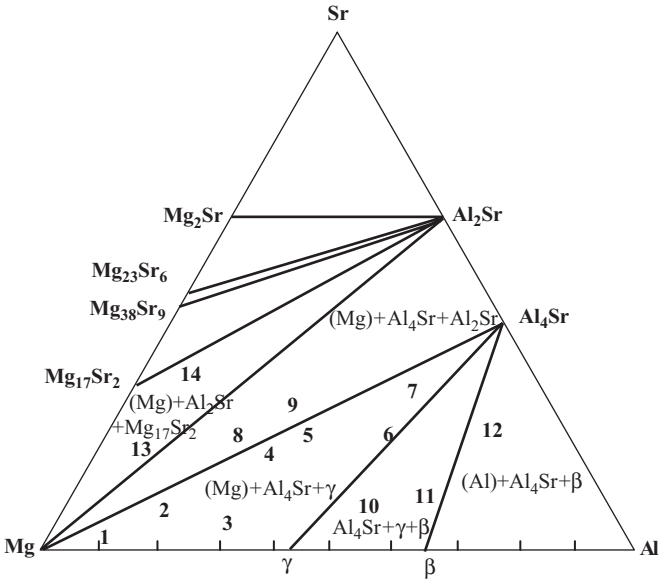

Fig. 1. Mg–Al–Sr ternary isothermal section at 25 °C showing the investigated compositions in wt% based on the thermodynamic modeling of [14].

SEM/EDS and EPMA were used to examine the phase compositions in the studied alloys. Chemical composition of the phases was determined using a CAMECA SX51 EPMA by which the measurements were carried out on three locations for each phase and the average was used in the present analysis. To limit the electron-specimen interaction volume, a relatively low acceleration voltage was used for the analysis because some of the phases occur in relatively small morphologies. Pure Mg and Al_4Sr standards were used for the EPMA quantitative analysis. Furthermore, to assure the homogeneity, the samples were taken from different locations in the castings and identical phase transformations using DSC were observed. The melting enthalpy of these samples was very similar. Morphologies of the same compositions at different locations from the castings were found similar.

The solidification curves established from the DSC measurements are based on the heat transfer between the sample and the reference as shown by Tian equation [20,21]. Heat flow produced inside the sample (reaction, transition) can be written as

$$\phi_r = -\phi - (C_s - C_r)\frac{dT_r}{dt} - R_{fs}C_s\frac{d\phi}{dt}, \quad (1)$$

where $\phi = \phi_{fr} - \phi_{fs}$ is the heat flow difference between the sample and the reference which is directly measured by the DSC, t is the time, R_{fs} and C_s are the heat transfer resistance and heat capacity of the sample. The second term,$(C_s - C_r)(dT_r/dt)$, takes the asymmetry in the heat capacities of the sample and reference into account and is assumed negligible. This assumption is valid because the DSC curve is adjusted so that the baseline is flat. The third term considers the contribution of the thermal inertia of the system.

The heat flow generated by a reaction or phase transformation in the sample ϕ_r can be expressed by the heat evolution, h, which occurs in the sample: $\phi_r = dh/dt$. Chen et al. [22] assumed a linear dependence of the rate of heat evolution during solidification on the rate of solid-phase fraction, $dh/dt = H(d(1-f_l)/dt)$, the total latent heat of solidification, H, is assumed to be constant. Eq. (1) can be rewritten as

$$H\frac{d(1-f_l)}{dt} = -\phi - RC\frac{d\phi}{dt}. \quad (2)$$

The terms H and RC were treated as adjustable parameters determined from the measured DSC curve of the sample. H is obtained by integration of the area under DSC curve after the baseline was subtracted, and the term RC, time constant τ of the DSC, is iteratively obtained from the after reaction part of the DSC curve because there is no reaction heat input or output in the sample cell then [23].

3. Results and discussions

3.1. Samples in the Mg+Al_4Sr+γ-phase field

Composition 1 (3.32/87.29/9.39 Sr/Mg/Al wt%) is located close to the Mg-rich corner in the primary precipitation field of Mg and in the Mg + Al_4Sr + γ-phase field as can be seen in Figs. 1. Fig. 2 shows the SEM image, EPMA analysis and solidification curve of this composition. SEM image indicates that: (i) the matrix region (A) contained magnesium and small amount of aluminum; (ii) the grain boundary region (B) contained magnesium as well as aluminum and strontium. Table 2 summarizes the compositions and the phases at room temperature identified by SEM/EDS, EPMA and XRD analyses. Two phases, (Mg) and (Al_4Sr), were positively identified in the microstructure. SEM image shows that the dark Mg-matrix phase was separated by bright precipitates and the grain boundary network is not continuous. The network is connected via Mg-matrix bridges. $Mg_{17}Al_{12}$ (γ) phase was not identified positively in the XRD pattern. The (Al_4Sr) phase is located at the grain boundary region and appears to be lamellae. The AJ51x, AJ62x and AJ62Lx alloys developed by Noranda also showed this phase [11]. Large ternary solid solubility was observed in this alloy. Quantitative EPMA analysis in Fig. 2(IV) shows that Mg dissolves 4.8 at% Al, whilst the Al_4Sr dissolves 23.2 at% Mg. It is worth noting, as can be seen in Fig. 2(III), that the solidification curve deduced from the DSC measurement shows that (Mg) starts to solidify at 602 °C consuming 67 wt% of the liquid and, binary and ternary invariant reactions occur at 517 and 525 °C, respectively, precipitating (Mg) and (Al_4Sr) from the remaining liquid at the grain boundary of the Mg-matrix as can be seen in Fig. 2(I). A very good agreement between the SEM/EDS, XRD and EPMA analyses was observed in terms of phase identification.

Spot analysis of composition 2 (8.65/76.15/15.20 Sr/Mg/Al wt%) was carried out at two different locations as shown in Fig. 3. The microstructure is characterized as dendrites and two types of secondary phases were observed. Both types of secondary phases contain all the three elements; Mg, Al and Sr. The eutectic morphology is more evident in this alloy than in composition 1 as shown in Fig. 3(II). Moreover, the solidification curve, as can be seen in Fig. 3(III), shows that (Mg) starts to solidify at 530 °C down to 516 °C consuming more than 17 wt% of the liquid, (Mg) and (Al_4Sr) precipitate at 516 °C then a ternary invariant reaction occurs at 507 °C precipitating (Mg), (Al_4Sr) and ($Mg_{17}Sr_2$) consuming the remaining liquid. It can be seen by the EPMA analysis, as shown in Fig. 3 and Table 2, that the dark phase is Mg dissolving 7.4 at% Al and the gray bulky phase is $Mg_{17}Sr_2$ dissolving 19.3 at% Al. Al_4Sr was predicted by the thermodynamic calculation of this alloy and confirmed by the XRD measurement but due to the small size of the precipitates it was difficult to detect this phase using EPMA.

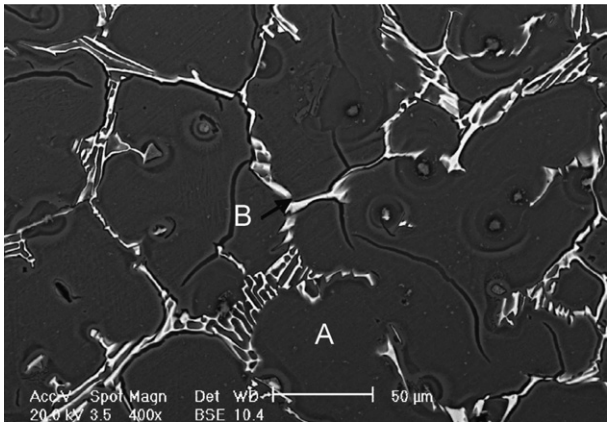

(I)

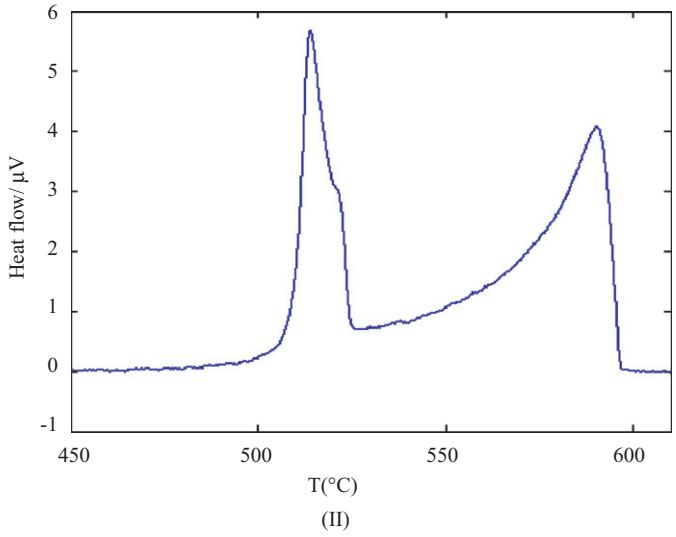

(II)

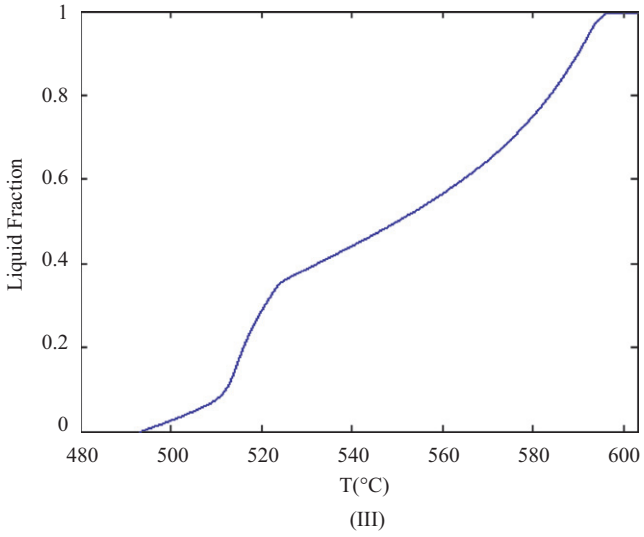

(III)

Location	at.% Mg	at.% Al	at.% Sr	Phases
A	95.2	4.8	0.0	(Mg)
B	23.2	58.2	18.6	(Al_4Sr)

(IV)

Fig. 2. (I) SEM image; (II) DSC spectra; (III) Solidification curve and (IV) EPMA analysis of composition 1.

Table 2
Composition and room temperature phase content of the investigated samples in the Mg + Al_4Sr + γ phase field

Composition				Identified phases		Solubilities (at%) (EPMA)
No.	Wt%			EPMA and SEM/EDS	XRD [19]	
	Sr	Mg	Al			
1	3.32	87.29	9.39	(Mg) and (Al_4Sr)	(Mg) and (Al_4Sr)	Mg dissolves 4.8 at% Al and Al_4Sr dissolves 23.2 at% Mg
2	8.65	76.15	15.20	(Mg) and ($Mg_{17}Sr_2$)	(Mg) and (Al_4Sr)	Mg dissolves 7.4 at% Al, $Mg_{17}Sr_2$ dissolves 19.3 at% Al
3	6.88	65.45	27.67	(Mg), (Al_4Sr) and γ	(Mg), (Al_4Sr) and γ	Mg dissolves 11.4 at% Al, Al_4Sr dissolves 7.9 at% Mg.
4	22.48	48.57	28.95	(Al_4Sr) and γ	(Mg), (Al_4Sr) and γ	Al_4Sr dissolves 10.8 at% Mg
5	22.53	43.75	33.72	(Mg), (Al_4Sr) and γ	(Mg), (Al_4Sr) and γ	Mg dissolves 10.6 at% Al, Al_4Sr dissolves 9.2 at% Mg
6	24.00	30.00	46.00	(Al_4Sr) and γ	(Al_4Sr), γ and τ	Al_4Sr dissolves 4.9 at% Mg
7	32.00	22.00	46.00	(Al_4Sr) and γ	(Al_4Sr) and γ	Al_4Sr dissolves 5.1 at% Mg

In the present EPMA analysis, the large precipitate (spot B) shown in Fig. 3(IV) is identified as $Mg_{17}Sr_2$ dissolving 19.3 at% Al. Baril et al. [11] reported the existence of a bulky phase with chemical composition 78.10 ± 1.18 at% Mg, 4.58 ± 0.37 at% Sr and 17.32 ± 0.99 at% Al in AJ52x alloy. This is not close to the chemical composition of the

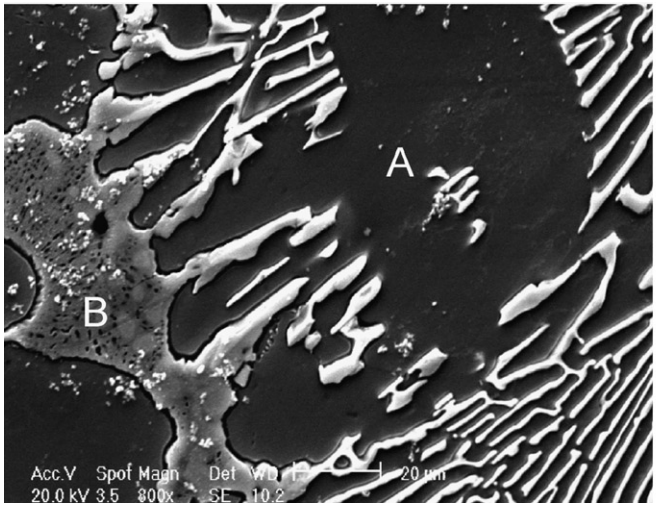

(I)

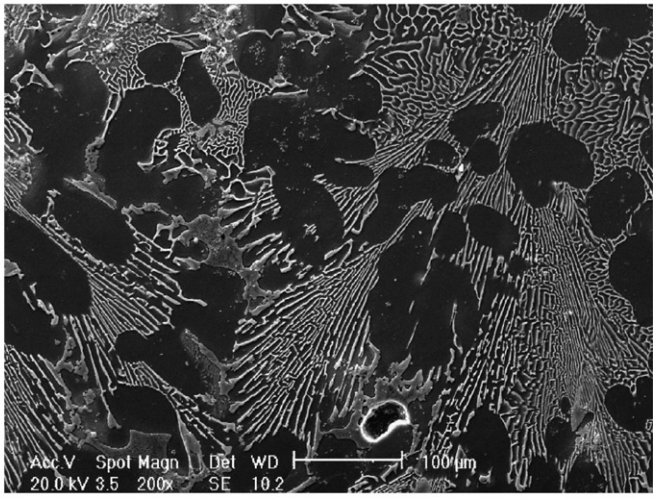

(II)

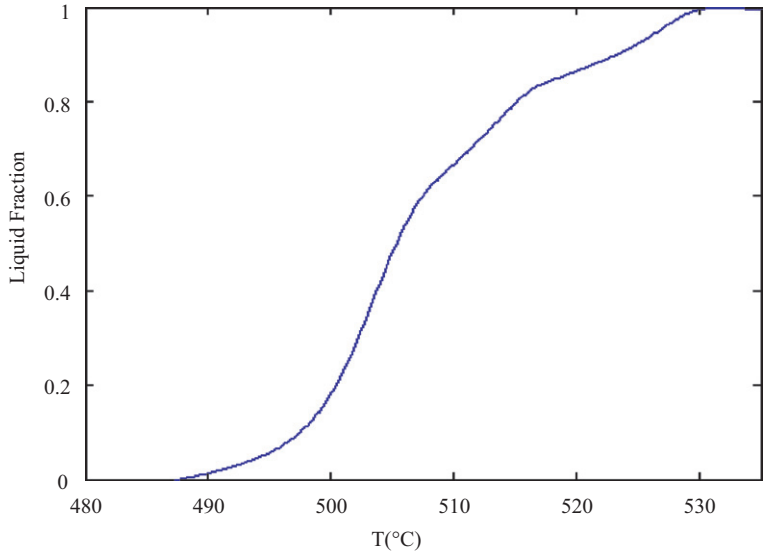

(III)

Location	at.% Mg	at.% Al	at.% Sr	Phases
A	92.6	7.4	0.0	(Mg)
B	71.4	19.3	9.3	($Mg_{17}Sr_2$)

(IV)

Fig. 3. SEM image (I) 800 ×; (II) 200 ×; (III) solidification curve and (IV) EPMA analysis of composition 2.

large precipitate observed in sample 2. However, the stoichiometry of this bulky phase was not clearly identified and they [11] tentatively designated the phase as $Al_3Mg_{13}Sr$. According to the current research, the extent of the ($Mg_{17}Sr_2$) phase field in the calculated ternary Mg–Al–Sr system reported by [14] and [15] is predicted narrower than what it should be and thus the system needs to be re-optimized.

Fig. 4 shows SEM image, EPMA analysis at three different spots and solidification curve of composition 3 (6.88/65.45/27.67 Sr/Mg/Al wt%). The plate-like phase is identified as (Al_4Sr) while the darker phase is designated as (Mg) according to the EPMA and XRD analysis as summarized in Table 2. γ-phase detected in region (C) was identified positively in both XRD and EPMA analyses. Ternary solid solubility was measured by quantitative EPMA analysis. It can be seen in Fig. 4(II) that Mg dissolves 11.4 at% Al whilst the binary compound Al_4Sr dissolves 7.9 at% Mg. A very small amount of Sr was detected in region (C) and negligible amount in region (B). Moreover, the solidification curve of sample 3 in Fig. 4(III) shows three-phase transformations: first occurs at 525 °C forming (Al_4Sr) consuming around 10 wt% of the liquid, second at 472 °C forming (Al_4Sr) and (Mg) and the third one at 429 °C precipitating (Al_4Sr), (Mg) and γ from the remaining liquid.

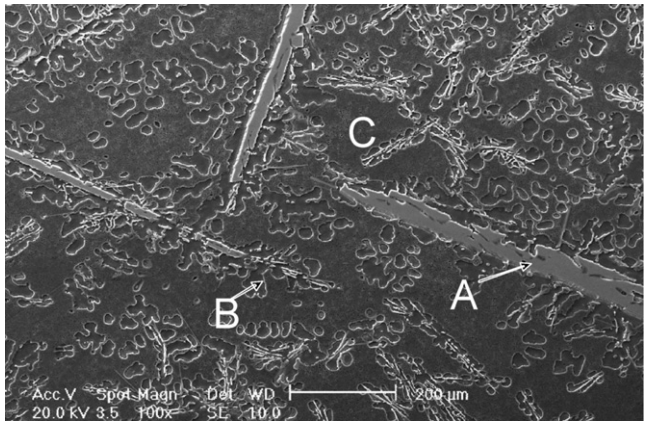

(I)

Location	at.% Mg	at.% Al	at.% Sr	Phases
A	7.9	70.3	21.0	(Al_4Sr)
B	88.6	11.4	0.0	(Mg)
C	59.2	40.6	0.2	γ

(II)

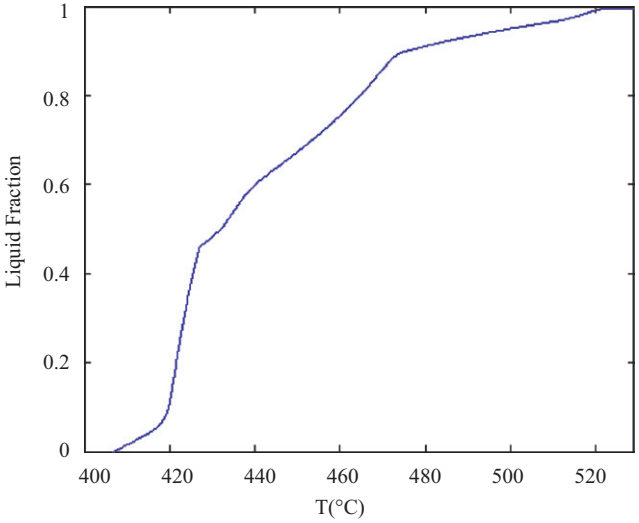

(III)

Fig. 4. (I) SEM image; (II) EPMA analysis and (III) solidification curve of composition 3.

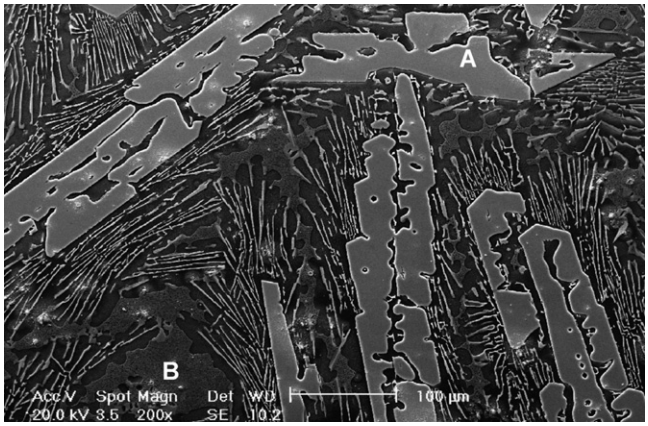

(I)

Location	at.% Mg	at.% Al	at.% Sr	Phases
A	10.8	68.3	20.9	(Al_4Sr)
B	63.4	36.3	0.3	γ

(II)

Fig. 5. (I) SEM image and (IV) EPMA analysis of composition 4.

Composition 4 (22.48/48.57/28.95 Sr/Mg/Al wt%) has plate-like structure, eutectic morphology and dark matrix as shown in Fig. 5. SEM/EDS analysis indicates that: (i) the plate-like phase in region (A) contains Al, Sr and Mg, (ii) region (B) contains Mg and Al, and (iii) the eutectic region contains all three elements. The plates are larger than those observed in composition 3. It can be seen in Table 2 that both (Mg), (Al_4Sr) were identified by XRD and EPMA analyses whereas γ phase was not detected in the XRD pattern. In this sample, Al_4Sr dissolves 10.8 at% Mg as shown in Fig. 5(II). A very negligible amount of Sr was detected in region (B) by EPMA analysis.

Composition 5 (22.53/43.75/33.72 Sr/Mg/Al wt%) is located very close to the boundary of two three-phase regions; $Mg + Al_4Sr + \gamma$ and $Mg + Al_4Sr + Al_2Sr$ as shown in Fig. 1. It can be seen in Fig. 6(I) that the amount of plate-like phase is relatively higher than in composition 2 and 4. This phase is identified as (Al_4Sr) by XRD and EPMA analyses as shown in Table 2 and Fig. 6(II), respectively. Besides, the solidification curve of sample 5 in Fig. 6(III) shows that formation of (Al_4Sr) consumed more than 60 wt% of the liquid, this is evident from the relative amount shown in the SEM image in Fig. 6(I). γ-phase is identified in region (B), which appeared with higher contents in alloy 5 than in alloy 4. The matrix in region (C) was identified as (Mg) and supported by XRD analysis as shown in Table 2. A very good agreement between XRD and EPMA analyses was observed.

Composition 6 (24/30/46 Sr/Mg/Al wt%) is located faraway from Mg-rich region and very close to the boundary of two three-phase regions; $Mg + Al_4Sr + \gamma$ and $Al_4Sr + \gamma + \beta$. In the XRD and EPMA analyses, γ and (Al_4Sr) were identified positively as shown in Table 2 and Fig. 7(II). Here, Al_4Sr dissolves 4.9 at% Mg. In addition, SEM/EDS analysis indicated that the plate-like phase has the three elements; Al, Sr and a very small amount of Mg, whereas region (B) contained Mg and Al. Also, some distinct peaks that are not associated with the known phases in the Mg–Al–Sr system have been observed in the XRD pattern and tentatively designated as τ, a ternary compound or solid solution, which is, however, not being identified and confirmed by EPMA analysis in the microstructure.

SEM image and EPMA analysis of composition 7 (32/22/46 Sr/Mg/Al wt%) are shown in Fig. 8. The plate-like phase is identified as Al_4Sr which dissolves 5.1 at% Mg and the region B is identified as γ. It is apparent that the amount of solid solution increases as the composition gets

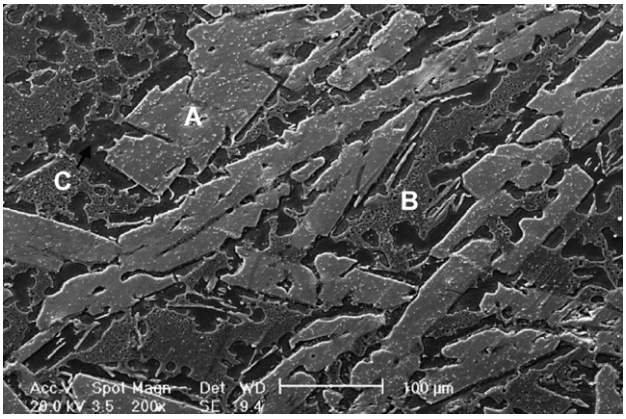

(I)

Location	at.% Mg	at.% Al	at.% Sr	Phases
A	9.2	69.8	21.0	(Al_4Sr)
B	61.3	38.6	0.1	γ
C	89.4	10.6	0.0	(Mg)

(II)

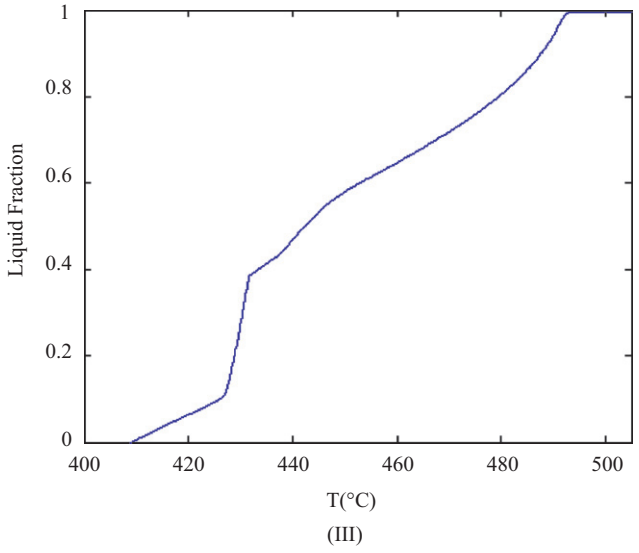

(III)

Fig. 6. (I) SEM image; (II) EPMA analysis and (III) solidification curve of composition 5.

closer to Al_4Sr compound. The solubility of Sr in γ was also found negligible in this alloy.

3.2. Samples in the Mg+Al_4Sr+Al_2Sr phase field

It can be seen in Fig. 1 that composition 8 (22.78/54.39/22.83 Sr/Mg/Al wt%) is located in the Mg-rich corner close to composition 4, but the two alloys belong to two different phase fields. SEM image as shown in Fig. 9(I) shows that the size of the plate-like phase is relatively smaller than in alloy 4 and it is distributed more evenly in the microstructure. Table 3 summarizes the compositions and room temperature phase contents identified by EPMA, SEM/EDS and XRD for the samples in this phase field. (Mg), (Al_4Sr) and ($Mg_{17}Sr_2$) were identified in the diffraction patterns and by the EPMA analysis of regions (A), (B) and

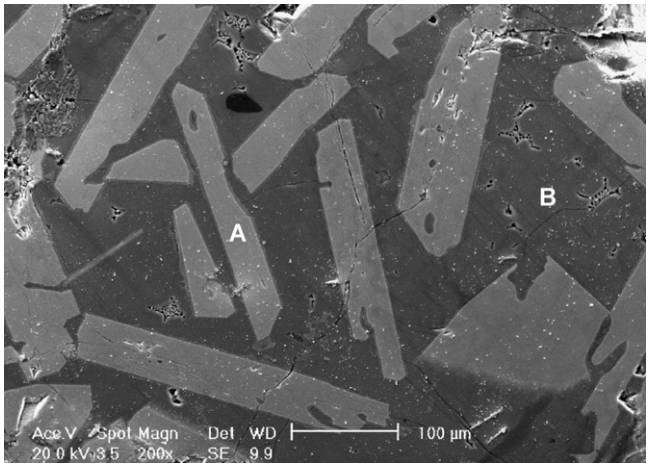

(I)

Location	at.% Mg	at.% Al	at.% Sr	Phases
A	4.9	74.0	21.1	(Al_4Sr)
B	56.5	43.4	0.1	γ

(II)

Fig. 7. (I) SEM image and (II) EPMA analysis of composition 6.

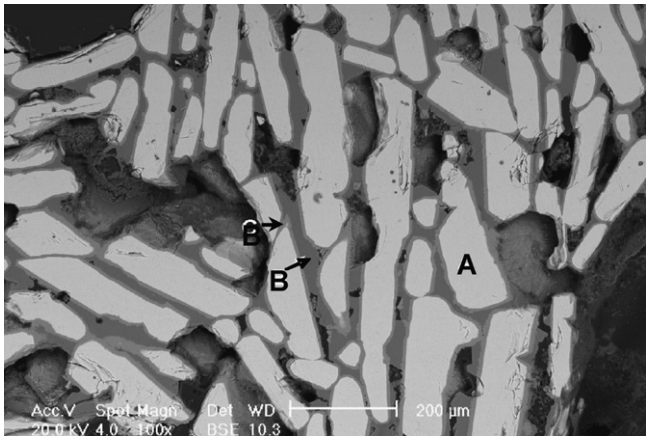

(I)

Location	at.% Mg	at.% Al	at.% Sr	Phases
A	5.1	74.5	20.4	(Al_4Sr)
B	57.5	42.4	0.1	γ

(II)

Fig. 8. (I) SEM image and (II) EPMA analysis of composition 7.

(C), respectively, as shown in Fig. 9(I). From the EPMA analysis shown in Fig. 9(II), Al_4Sr dissolves 14.1 at% Mg. In contrast, 10.8 at% of Mg is dissolved in Al_4Sr in alloy 4. In the present EPMA analysis, the light gray precipitate is identified as $Mg_{17}Sr_2$ dissolving 21.3 at% Al, which is the maximum observed solubility of Al in $Mg_{17}Sr_2$. Moreover, sample 8 is located in the three phase, (Mg), (Al_4Sr) and ($Mg_{17}Sr_2$), region which was, however, not predicted correctly by [14,15] as shown in Fig. 1(I). The composition

of the light gray phase is also not close to that of $Al_3Mg_{13}Sr$ observed by Baril et al. [11].

In Fig. 9(III), the solidification curve shows that (Al_4Sr) starts to solidify at 613 °C down to 544 °C consuming 23 wt% of the liquid and, at 544 °C (Al_4Sr) and (Mg) are forming. Finally a ternary invariant point occurs at 513 °C forming (Al_4Sr), (Mg) and ($Mg_{17}Sr_2$).

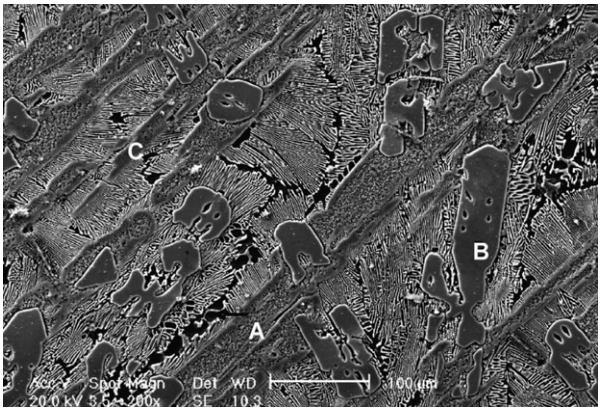

(I)

Location	at.% Mg	at.% Al	at.% Sr	Phases
A	88.6	11.2	0.2	(Mg)
B	14.1	64.5	21.4	(Al_4Sr)
C	70.0	21.3	8.7	($Mg_{17}Sr_2$)

(II)

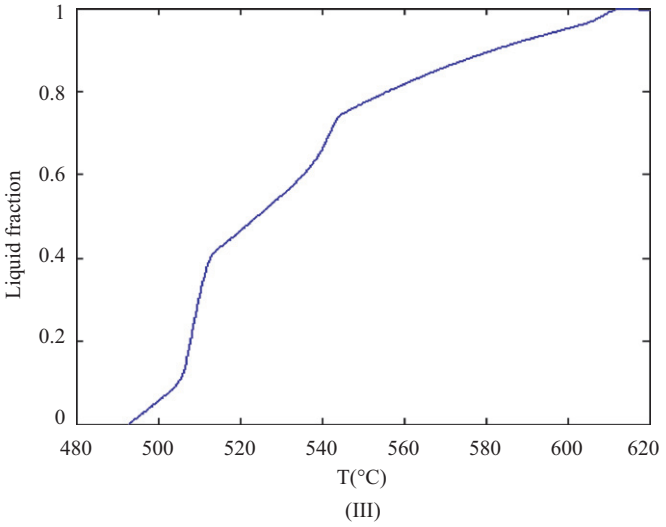

(III)

Fig. 9. (I) SEM image; (II) EPMA analysis and (III) solidification curve of composition 8.

Composition 9 (27.83/42.89/29.28 Sr/Mg/Al wt%) is located in the same three-phase region as composition 8. SEM image, EPMA analysis and solidification curve are shown in Fig. 10. The microstructure of alloys 8 and 9 appeared to be quite similar. It is a plate-like structure with dark and light-gray phases. It can be seen in Table 3 that (Mg), (Al_4Sr) and ($Mg_{17}Sr_2$) have been identified in the XRD pattern; however, with the EPMA analysis only (Al_4Sr) and ($Mg_{17}Sr_2$) have been identified. The plate-like phase has been identified as Al_4Sr that dissolves 12.5 at% Mg. According to the EPMA analysis shown in Fig. 10(II), the light gray phase in region (B) is $Mg_{17}Sr_2$ dissolving 20.2 at% Al. Similar ternary solid solubility has been observed in composition 8. It is obvious from the above discussion that a ternary solid solubility of $Mg_{17}Sr_2$ has been formed in the studied alloys and the phase region was not predicted correctly by [14,15]. According to the current understanding of the Mg–Al–Sr system, this sample is located in the three-phase region of (Mg), (Al_4Sr) and ($Mg_{17}Sr_2$). It is worth noting, as shown in Fig. 10(III), that the solidification curve shows that (Al_4Sr) start to solidify at 600 °C down to 445 °C consuming around 10 wt% of the liquid, binary and ternary invariant reactions occur, respectively, at 545 and 512 °C precipitating (Al_4Sr), ($Mg_{17}Sr_2$) and γ from the remaining liquid.

3.3. Samples in the $Al_4Sr+\gamma+\beta$ phase field

Table 4 summarizes the results of the investigated samples in this phase field. Fig. 11 shows SEM image and EPMA analysis of composition 10 (9.5/40/50.5 Sr/Mg/Al wt%). The microstructure of this alloy exhibits different morphology where the plate-like phase appears thinner. The XRD and EPMA analyses, shown in Table 4 and Fig. 11(II), respectively, identified (Al_4Sr) and β positively. In the XRD pattern, γ had a very small volume fraction and it was also not identified in the EPMA analysis. In this sample, Al_4Sr phase dissolves 4.0 at% of Mg as shown in Fig. 11(II).

SEM image and EPMA analysis of composition 11 (11/30/59 Sr/Mg/Al wt%) are shown in Fig. 12. The

Table 3
Composition and room temperature phase content of the investigated samples in the Mg + Al_4Sr + Al_2Sr phase field

Composition				Identified phases		Solubilities (at%) (EPMA)
No.	Wt%			EPMA and SEM/EDS	XRD [19]	
	Sr	Mg	Al			
8	22.78	54.39	22.83	(Mg), (Al_4Sr) and ($Mg_{17}Sr_2$)	(Mg), (Al_4Sr) and ($Mg_{17}Sr_2$)	Mg dissolves 11.2 at% Al, Al_4Sr dissolves 14.1 at% Mg and $Mg_{17}Sr_2$ dissolves 21.3 at% Al
9	27.83	42.89	29.28	(Al_4Sr) and ($Mg_{17}Sr_2$)	(Mg), (Al_4Sr) and ($Mg_{17}Sr_2$)	Al_4Sr dissolves 12.5 at% Mg and $Mg_{17}Sr_2$ dissolving 20.2 at% Al

microstructure is characterized by thick and thin plate-like structures and both of them have similar chemistry. The XRD analysis as reported in Table 4 identified three phases: (Al_4Sr), γ and β. The EPMA analysis, however, confirmed the existence of two phases (Al_4Sr) and β. It was observed that Al_4Sr dissolves 2.1 at% of Mg in both regions (A) and (C) as can be seen in Fig. 12(II).

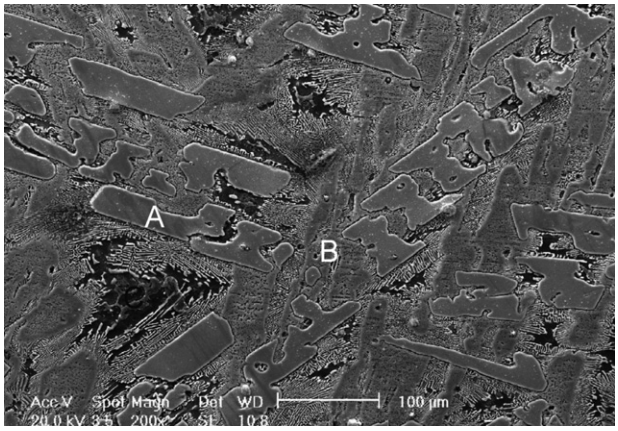

(I)

Location	at.% Mg	at.% Al	at.% Sr	Phases
A	12.5	66.6	20.9	(Al_4Sr)
B	70.6	20.2	9.2	($Mg_{17}Sr_2$)

(II)

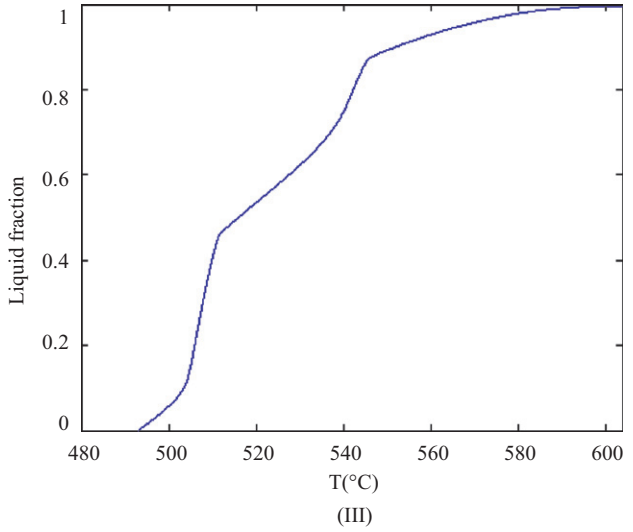

(III)

Fig. 10. (I) SEM image; (II) EPMA analysis and (III) solidification curve of composition 9.

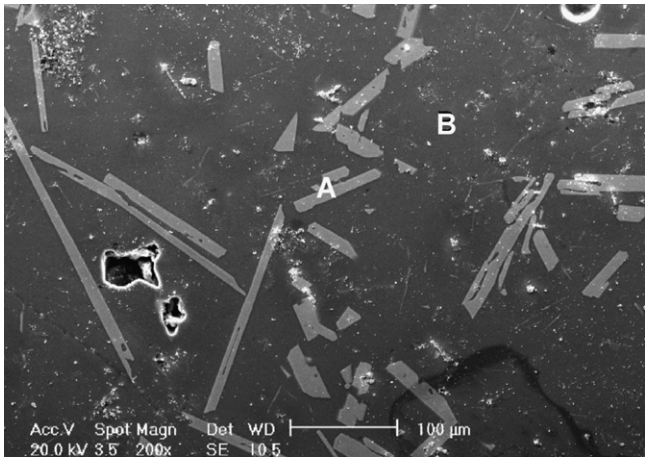

(I)

Location	at.% Mg	at.% Al	at.% Sr	Phases
A	4.0	75.4	20.6	(Al_4Sr)
B	49.1	50.7	0.2	β

(II)

Fig. 11. (I) SEM image and (II) EPMA analysis of composition 10.

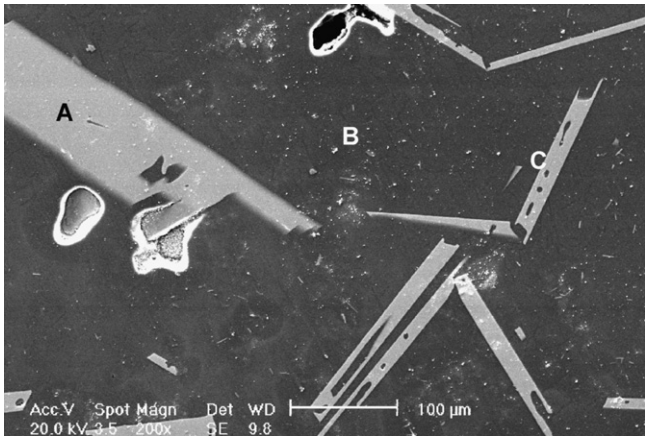

(I)

Location	at.% Mg	at.% Al	at.% Sr	Phases
A	2.1	77.0	20.9	(Al_4Sr)
B	38.9	61.1	0.0	β
C	2.1	76.8	21.1	(Al_4Sr)

(II)

Fig. 12. (I) SEM image and (II) EPMA analysis of composition 11.

Table 4
Composition and room temperature phase content of the investigated samples in the $Al_4Sr+\gamma+\beta$ phase field

Composition				Identified phases		Solubilities (at%) (EPMA)
No.	Wt%			EPMA and SEM/EDS	XRD [19]	
	Sr	Mg	Al			
10	9.50	40.00	50.50	(Al_4Sr) and β	(Al_4Sr), γ and β	Al_4Sr dissolves 4.0 at% Mg
11	11.00	30.00	59.00	(Al_4Sr) and β	(Al_4Sr), γ and β	Al_4Sr dissolves 2.1 at% Mg

3.4. $Al+Al_4Sr+\beta$ phase field

Fig. 13 and Table 5 show SEM/EDS, XRD pattern and EPMA analyses of composition 12 (23/15/62 Sr/Mg/Al wt%). The plate-like phase became thicker and larger as the alloy becomes closer to the Al_4Sr-rich region. Regions (A) and (B) were identified as (Al_4Sr) and β by EPMA analysis which was supported by the XRD results as shown in Table 5 and Figs. 13(II). (Al) was identified only in the XRD pattern as the microprobe analysis was conducted only in the two distinct regions of the micrograph shown in Fig. 13(I). Quantitative EPMA analysis shows that Al_4Sr dissolves 1.7 at% Mg, whilst the β phase does not show any solubility of Sr. In all the three alloys which contained β phase, no or negligible solubility of Sr was detected by the EPMA analysis.

3.5. Samples in the $Mg+Al_2Sr+Mg_{17}Sr_2$ phase field

SEM image and EPMA analyses of composition 13 (19.9/72.0/8.1 Sr/Mg/Al wt%) are shown in Fig. 14. The microstructure is characterized as very bulky phase surrounded by (Mg) matrix. XRD and EPMA analyses, as reported in Table 6, identified both (Mg) and ($Mg_{17}Sr_2$). According to SEM and EPMA analyses the dark phase was identified as Mg, which dissolves 5.0 at% Al. The large precipitates are identified as $Mg_{17}Sr_2$ that dissolves 8.5 at% Al.

Fig. 15 shows SEM/EDS at two different spots and EPMA analyses of composition 14 (32.74/60.55/6.71Sr/Mg/Al wt%). Two phases have been identified positively by XRD in sample 14 as shown in Table 6. EPMA analysis identified the phases in regions (A) and (B) as ($Mg_{17}Sr_2$) and ($Mg_{38}Sr_9$), respectively, as shown in Fig. 15(II). SEM/EDS analysis indicates that both regions (A) and (B) contain all the three elements; Mg, Al and Sr. In this alloy, EPMA analysis shows that $Mg_{17}Sr_2$ dissolves 6.4 at% Al and $Mg_{38}Sr_9$ dissolves 12.5 at% Al. This suggests, also, that the extent of the ($Mg_{38}Sr_9$) phase field in the ternary Mg–Al–Sr system is predicted narrower in the calculated phase diagrams reported in Refs. [14,15] and thus the system needs to be re-optimized.

Based on the experimental results presented in this article, a new Mg–Al–Sr isothermal section at 300 K was drawn and compared with that calculated from the thermodynamic modeling of [14]. It can be seen in Fig. 16 that the extended solubility of the binary

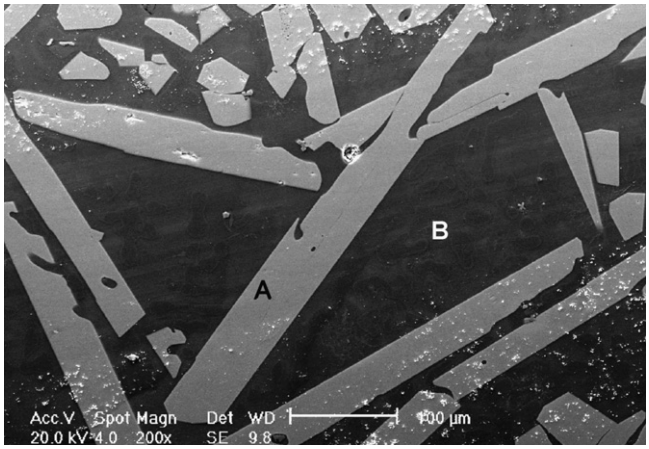

(I)

Location	at.% Mg	at.% Al	at.% Sr	Phases
A	1.7	77.2	21.1	(Al_4Sr)
B	37.4	62.5	0.0	β

(II)

Fig. 13. (I) SEM image and (II) EPMA analysis of composition 12.

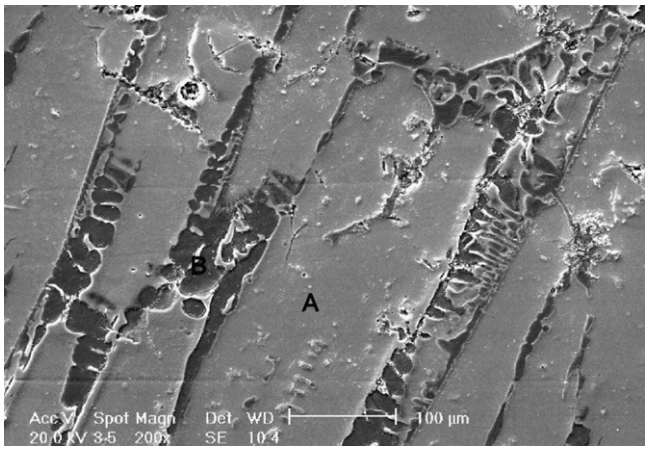

(I)

Location	at.% Mg	at.% Al	at.% Sr	Phases
A	81.7	8.5	9.8	($Mg_{17}Sr_2$)
B	94.9	5.0	0.1	(Mg)

(II)

Fig. 14. (I) SEM image and (II) EPMA analysis of composition 13.

Table 5
Composition and room temperature phase content of the investigated sample in the $Al+Al_4Sr+\beta$ phase field

Composition				Identified phases		Solubilities (at%) (EPMA)
No.	Wt%			EPMA and SEM/EDS	XRD [19]	
	Sr	Mg	Al			
12	23	15	62	(Al_4Sr) and β	(Al), (Al_4Sr) and β	Al_4Sr dissolves 1.7 at% Mg

Table 6
Composition and room temperature phase content of the investigated samples in the (Mg) + Al_2Sr + $Mg_{17}Sr_2$ phase field

Composition				Identified phases		Solubilities (at%) (EPMA)
No.	Wt%			EPMA and SEM/EDS	XRD [19]	
	Sr	Mg	Al			
13	19.90	72	8.1	(Mg) and ($Mg_{17}Sr_2$)	(Mg) and ($Mg_{17}Sr_2$)	Mg dissolves 5.0 at% Al and $Mg_{17}Sr_2$ dissolves 8.5 at% Al.
14	32.74	60.55	6.71	($Mg_{17}Sr_2$) and ($Mg_{38}Sr_9$)	($Mg_{17}Sr_2$) and ($Mg_{38}Sr_9$)	$Mg_{17}Sr_2$ dissolves 6.4 at% Al and $Mg_{38}Sr_9$ dissolves 12.5 at% Al

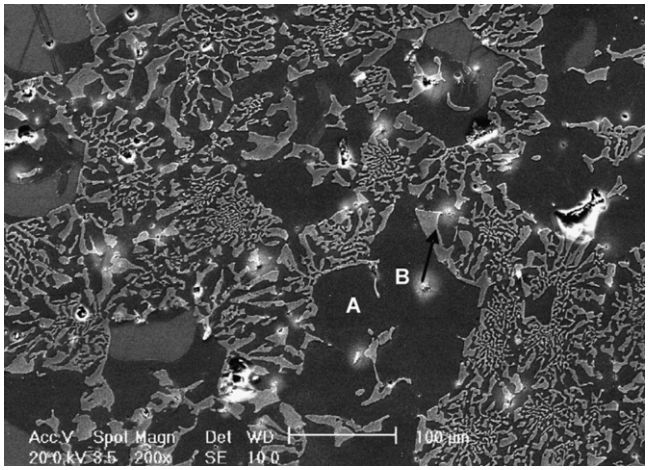

(I)

Location	at.% Mg	at.% Al	at.% Sr	Phases
A	83.0	6.4	10.6	($Mg_{17}Sr_2$)
B	70.8	12.5	16.7	($Mg_{38}Sr_9$)

(II)

Fig. 15. (I) SEM image and (II) EPMA analysis of composition 14.

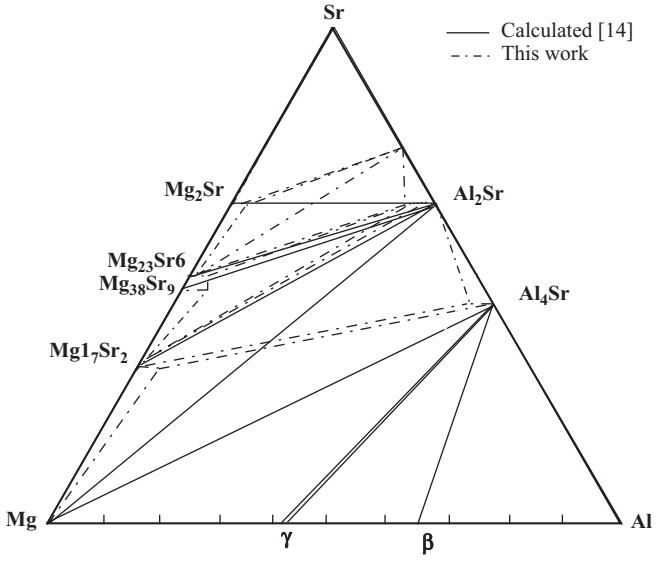

Fig. 16. Mg–Al–Sr isothermal section at 300 K.

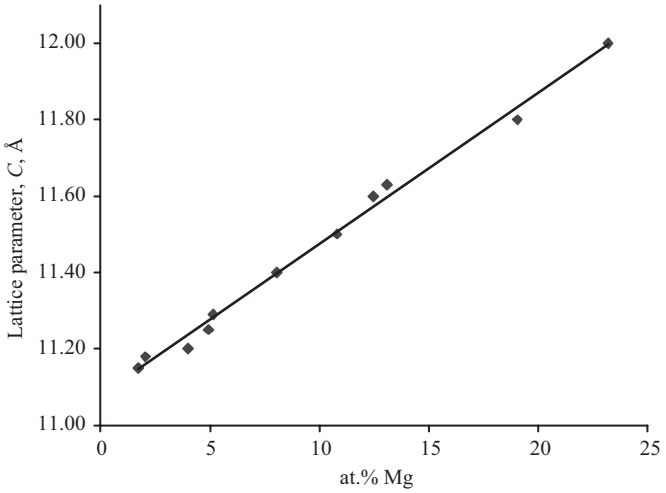

Fig. 17. Lattice parameter, C, of the $Mg_xAl_{4-x}Sr$ solid solution versus Mg content.

compounds, observed in this work, resulted in significant deviation between the two isothermal sections.

3.6. Solubility limit of the ternary solid solution $Mg_xAl_{4-x}Sr$

A solid solution of Mg in Al_4Sr was detected by XRD as well as EPMA. Solid solubility up to 23.2 at% Mg in the Al_4Sr compound was detected in the investigated samples. Lattice parameter, as shown in Fig. 17, increases linearly with Mg content as does the unit cell volume. The relation between lattice parameter C and Mg content is represented in Eq. (3), which describes the experimental data well with a coefficient of determination, R^2, 99.34%. Such a behavior was expected considering the similar atomic sizes of Mg and Al; the atomic radius of Mg is 0.160 nm against 0.143 nm for Al, i.e., an increase of about 11%.

$$C(x) = 0.039x + 11.082. \quad (3)$$

From the above equation, the extrapolated value at $x = 0.0$ is $C = 11.082$ Å. The experimental C lattice parameter of the Al_4Sr have been reported as $C = 11.07$ Å [24]. This excellent agreement between the extrapolated and measured values confirms that the lattice parameter, C, of the $Mg_xAl_{4-x}Sr$ solid solution increases linearly with Mg content, x, obeying Vegard's law in the investigated

samples. This solid solution is not a separate phase but it is due to the substitution of Al by Mg atoms in the binary Al_4Sr. Moreover, the solid solution of Mg in Al_4Sr must be considered as substitutional solid solution because of the following reasons: (i) Al/Sr ratio is not constant as proven by the EPMA analysis of all the samples containing this phase, and (ii) the numerical simulation of the X-ray spectra assuming substitutional solid solution using PowderCell 2.3 [25] agrees well with the experimental spectra but not if the solution is assumed to be interstitial. Further, it was observed that the other lattice parameter, *a*, remained constant.

4. Concluding remarks

A microstructural characterization of ternary Mg–Al–Sr alloys using XRD, SEM/EDS and EPMA was carried out. In the present investigation, three ternary solid solubilities have been reported; (Al_4Sr), ($Mg_{17}Sr_2$) and ($Mg_{38}Sr_9$). The solid solution (Al_4Sr) is represented by $Mg_xAl_{4-x}Sr$, which has plate-like structure. The maximum solubility of Al in $Mg_{17}Sr_2$ in the studied samples was found to be 21.3 at%. It was also observed that $Mg_{38}Sr_9$ dissolved 12.5 at% Al. A very negligible solubility of Sr in β and γ-phase was detected by EPMA analysis. The extended solid solubility of the binary compounds agrees with the experimental isothermal section of the Mg–Al–Sr system at 300 K. This isothermal section shows a triangulation involving $Mg_{17}Sr_2$, Al_4Sr and Mg_2Sr.

Acknowledgments

This research was carried out with the support of NSERC and NATEQ grants, Canada. The authors wish to express their appreciation for this support.

References

[1] R. Gradinger, P. Stolfig, Proc. Mine. Metals Mater. Soc. (TMS), 2003, pp. 231.
[2] S. Das, JOM 55 (2003) 22.
[3] M. Pekguleryuz, E. Baril, P. Labelle, D. Argo, J. Adv. Mater. 35 (2003) 32.
[4] E. Baril, P. Labelle, A. Fischerworring-Bunk, SAE World Congress, 01-0659, 2004, pp.1845.
[5] A. Prince, N. Nikitina, A Comprehensive Compendium of Evaluated Constitutional Date and Phase Diagram, vol. 16, VCH, New York, 1988, pp. 413.
[6] M.M. Makhmudov, A.V. Vakhovob, T.D. Dzhuraev, I.N. Ganiev, Dokl. Akad. Nauk Tadzh. 23 (1980) 25.
[7] M.M. Makhmudov, A.V. Vakhovob, T.D. Dzhuraev, Dokl. Akad. Nauk Tadzh. 24 (1981) 435.
[8] M.M. Makhmudov, A.V. Vakhovob, T.D. Dzhuraev, Russ. Metall. 6 (1981) 209.
[9] M.M. Makhmudov, A.V. Vakhovob, T.D. Dzhuraev, Russ. Metall. 1 (1982) 122.
[10] M.M. Makhmudov, A.V. Vakhovob, I.N. Ganiev, Zavod. Lab. 48 (1982) 61.
[11] E. Baril, P. Labelle, M. Pekguleryuz, JOM 55 (2003) 34.
[12] B. Jing, S. Yangshan, X. Shan, X. Feng, Z. Tianbai, Mater. Sci. Eng. A. 419 (2006) 181.
[13] F. Czerwinski, A. Zielinska-Lipiec, Acta Mater. 53 (2005) 3433.
[14] P. Chartrand, A.D. Pelton, J. Phase Equilib. 5 (1994) 591.
[15] O. Koray, Ph.D. Thesis, The Pensylvania State University, 2004.
[16] Z.K. Liu, Y. Zhong, C. Wolverton, A.Y. Chang, Acta Mater. 52 (2004) 2739.
[17] M.A. Parvez, E. Essadiqi, M. Medraj, Proc. CSME Forum, 2004, pp.829.
[18] M.A. Parvez, X. Wang, E. Essadiqi, M. Medraj, Proc. Mine. Metals Mater. Soc.(TMS), 2005, pp.179.
[19] M.A. Parvez, M. Medraj, E. Essadiqi, A. Muntasar, G. Dénès, J. Alloys Compd. 402 (2005) 170.
[20] G.W. Hohne, W. Hemminger, H.J. Flammershiem, Differential Scanning Calorimetry: An Introduction for Practitioners, Springer, Berlin-Heidelberg, 1996.
[21] W. Hemminger, H. Cammenga, Methoden der Thermischen Analyse, Springer, Berlin-Heidelberg, 1989.
[22] S.W. Chen, C.C. Huang, Acta Mater. 44 (1996) 1955.
[23] A.P. Gray, in: R.S. Porter, J.F. Johnson (Eds.), Analytical Calorimetry, Plenum Press, New York, 1968, p. 209.
[24] P. Villars, Pearson's Handbook, Crystallographic Data for Intermetallic Phases, 1997.
[25] W. Kraus, G. Nolze, PowderCell for Windows, Version 2.3, Berlin Federal Institute for Materials Research and Testing, Berlin, Germany, ASM International, 1999.